$P_8O_{12}\cdot 2BH_3$ – The Borane Adduct of a New Molecular Phosphorus Oxide

Akbar Tellenbach,[a] and M. Jansen*[a]

Keywords: Phosphorus / Phosphorus oxides / Boranes / Cage compounds / Dimerization

$P_4O_6\cdot BH_3$, which readily forms from P_4O_6 and $Me_2S\cdot BH_3$ in a stoichiometric reaction, dimerizes spontaneously at –30 °C in a concentrated toluene solution resulting in the crystallization of $P_8O_{12}\cdot 2BH_3$ (**1**). The synthesis of **1** represents the first selective interconnection of molecular phosphorus chalcogenides leading to the formation of a new, flexible P_8O_{12} cage. The thermodynamic driving force for the dimerization reaction results from a gain of enthalpy due to enhanced P–O double-bond contributions and a relief of angular strain. In terms of kinetics, the behavior of $P_4O_6\cdot BH_3$, differing from that of other P_4O_6 derivatives, is caused by the low π-donor ability of BH_3 provoking a Michaelis–Arbuzov-like reactivity at the adjacent phosphorus atom and thus inducing cage opening. **1** was characterized by means of X-ray diffractometry (powder, single crystal), NMR spectroscopy (solution, solid), IR spectroscopy, Raman spectroscopy, and mass spectrometry. Mass spectrometric investigations suggest considerable BH_3 abstraction as well as an enhanced stability of $P_8O_{12}\cdot BH_3$ and P_8O_{12}, compared to **1**.

Introduction

The chemical behavior of P_4O_6, a molecular phosphorus oxide having an adamantane-like birdcage structure, seems to be rather ambivalent. On the one hand P_4O_6 reacts readily with electrophilic compounds resulting in the attachment of terminal atoms or groups to phosphorus atoms of the cage. The electrophilic addition gives rise to the formation of chalcogen derivatives P_4O_n ($n = 7-10$),[1−6] $P_4O_6S_n$ ($n = 1-4$),[7−10] $P_4O_6Se_n$ ($n = 1-4$),[11−14] and transition metal complexes like $P_4O_6[Ni(CO)_3]_n$ ($n = 1-4$),[15,16] $P_4O_6[Fe(CO)_4]_n$ ($n = 1-4$),[17,18] and $P_4O_6[M(CO)_5]$ (M = Cr, Mo, W).[19] On the other hand, ring-opening reactions are much more difficult to control and normally lead to complete degradation of the framework.[20−22] Among the few selective cage-opening reactions, known so far, there is the formation of P_4O_6NR (R = organic groups) by nitrene insertion and rearrangement of the cage structure, resulting in an adamantane-like P_4O_5N unit.[23−25] Although quantum chemical calculations for P_4O_6X (X = O, S, H^+, F^+, Cl^+, N^-)[26] indicate a strong dependence of the P−O cage bond lengths on the electronegativity of terminal atoms attached to the phosphorus atom, very similar geometrical parameters have been found for the P_4O_6 cages of P_4O_7,[2,3] P_4O_6S,[7] P_4O_6Se,[11] and $P_4O_6Fe(CO)_4$.[18] Up to now, this observation and the different behavior of P_4O_6NR in comparison with P_4O_6X (e.g. X = O, S, Se, etc.) are not completely understood.

In contrast to chalcogen atoms, the electrophilic addition of BH_3 is expected to affect the cage bonds in a different manner due to the reduced π-donor abilities of boron. For this reason we have tried to synthesize and characterize borane complexes of P_4O_6, the constitutions of which were previously studied by ^{31}P NMR spectra of solutions.[27−29] Thus far, a detailed investigation of these compounds in a pure state failed because of their high sensitivity and instability. During our recent attempts in crystallizing dissolved $P_4O_6\cdot BH_3$, we have achieved the first selective dimerization of phosphorus chalcogenides. The obtained product, $P_8O_{12}\cdot 2BH_3$ (**1**), is the bis(borane) adduct of a new molecular phosphorus oxide P_8O_{12}.[30]

Results and Discussion

Synthesis and Thermal Properties

Depending on the relative quantities, P_4O_6 readily forms $P_4O_6\cdot nBH_3$ ($n = 1-3$) when reacting with gaseous diborane in organic solvents at room temperature.[28,29] The reaction takes place in a sequential manner with the successive coordination of one, two, and three BH_3 groups. The chemical shifts, coupling constants, and splitting patterns, observed in ^{31}P NMR spectra, clearly indicate boron atoms being attached to phosphorus atoms.[28,29] If pure liquid P_4O_6 is used, electrophilic addition stops at the stage of $P_4O_6\cdot 2BH_3$ due to crystallization.[27] For practical reasons, we have chosen $Me_2S\cdot BH_3$ as a reagent. The first equivalent of $Me_2S\cdot BH_3$ reacts completely within an hour, giving mainly $P_4O_6\cdot BH_3$ with small amounts of $P_4O_6\cdot 2BH_3$, P_4O_7, P_4, and some residual P_4O_6. $Me_2S\cdot BH_3$ is less effective than B_2H_6. Thus, $P_4O_6\cdot BH_3$ and $P_4O_6\cdot 2BH_3$ are generated in a 1:2.5

[a] Max Planck Institute for Solid State Research
Heisenbergstr. 1, 70569 Stuttgart, Germany
Fax: (internat.) + 49-711/689-1502
E-Mail: m.jansen@fkf.mpg.de

ratio without any $P_4O_6 \cdot 3BH_3$, even if 4 equiv. of $Me_2S \cdot BH_3$ are applied. The NMR spectroscopic data of these compounds (see Exp. Sect.) are in good agreement with those described earlier.[28] After removing Me_2S and storing a highly concentrated solution of $P_4O_6 \cdot BH_3$ in toluene at −30 °C for a period of three months, cuboid crystals were recovered. Crystal structure determination, ^{31}P NMR spectroscopy, and mass spectrometry (see below) demonstrate that the crystallization product does not consist of the expected $P_4O_6 \cdot BH_3$, but of the corresponding dimer $P_8O_{12} \cdot 2BH_3$, (Scheme 1).

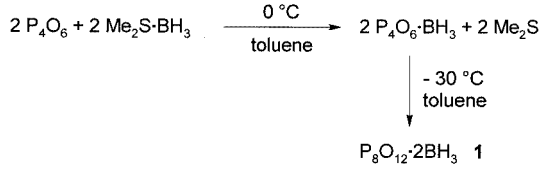

Scheme 1. Reaction scheme of the formation of **1**

Under standard conditions, **1** forms a colorless solid, which is extremely sensitive to humidity as well as to nucleophilic or protic reagents. Furthermore, **1** is highly explosive, when exposed to any kind of pressure, traces of pure water or ethanol. Upon heating the solid above 70 °C for some hours, decomposition occurs, with the color turning yellow, orange, and finally red. According to the results of temperature-dependent powder diffractometry (Guinier−Simon technique), crystalline BPO_4 (tetragonal) is generated above 230 °C. As is to be expected, the thermal decomposition is irreversible. Apart from a slight mass loss of about 4%, thermal analyses by DTA and TGA do not show any well-defined effect below 250 °C. In solution (toluene, xylene, CH_2Cl_2) **1** slowly decomposes furnishing a mixture of **1**, $P_4O_6 \cdot BH_3$, P_4O_6, and some P_4O_7. At room temperature the monomer/dimer ratio climbs to 1:1 within 18 h. Furthermore, the solution mainly contains entire molecules of **1**, even on heating at 70 °C for 2 h. On the other hand, $P_8O_{12} \cdot 2BH_3$ is stable at −30 °C both, as a solid and in solution.

Crystal Structure Determination

The powder diffraction pattern of **1** (Figure 1; Table 1) has been indexed based on an orthorhombic unit cell (Table 2). The crystal structure has been determined and refined using single-crystal X-ray methods. The crystal data are summarized in Table 2. A powder diffraction pattern, which has been calculated on the basis of the single-crystal data, is in good agreement with the observed one (Figure 1).

The crystal structure consists of $P_8O_{12} \cdot 2BH_3$ molecular units. As shown in Figure 2, two bicyclic $P_4O_5 \cdot BH_3$ subunits are connected by O1 and O7 in a way, such that the BH_3 groups are pointing in opposite directions (head−tail linkage). Thus, $P_8O_{12} \cdot 2BH_3$ represents the bis(borane) complex of a new molecular phosphorus oxide P_8O_{12}, which is the dimer of the well-known P_4O_6. In recent investigations concerning the dimerization tendency of molecular phosphorus oxides, we have been able to confirm the existence of ligand-free P_8O_{12} by means of ^{31}P NMR spectroscopy (P_8O_{12} has been mentioned before by Meisel and co-workers,[31] but neither experimental evidence nor analytical data were presented). Due to packing effects the point symmetry C_{2h}, expected for free $P_8O_{12} \cdot 2BH_3$ molecules, is reduced to C_1 in the crystalline solid. As a consequence, the two bicyclic $P_4O_5 \cdot BH_3$ units are folded and slightly twisted against each other (folding along the O1−O7 axis with torsion angles of 151° for P1−O1−O7−P5 and 164° for P4−O7−O1−P8; twisting along the O4−O10 axis; see Figure 2).

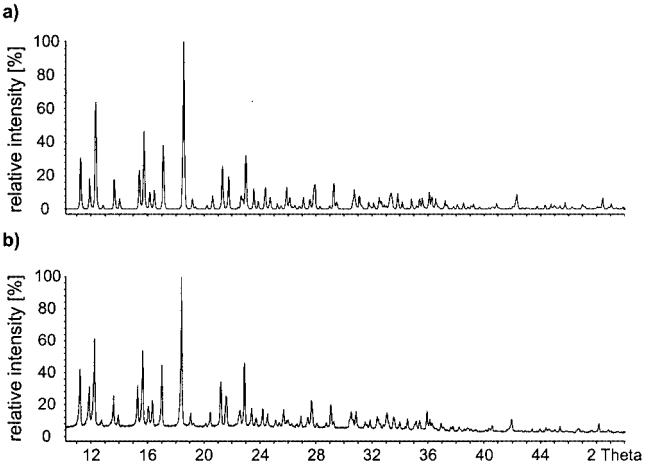

Figure 1. Powder diffraction pattern of **1**; calculated from single-crystal data (a) and observed (b)

Table 1. The 25 most intense reflections of the powder diffraction pattern of **1**; zero-point correction on the basis of silicon as external standard (a = 5.43088 Å[62])

$h\ k\ l$	2θ [°]	d [Å]	I_{rel} [%]
0 2 0	11.309	7.8178	41.7
0 2 1	11.948	7.4010	30.8
1 1 1	12.335	7.1697	61.1
0 2 2	13.688	6.4639	24.8
0 0 4	15.405	5.7471	32.0
1 2 1	15.772	5.6142	53.1
0 2 3	16.184	5.4722	18.2
1 1 3	16.473	5.3768	22.4
1 2 2	17.134	5.1709	43.7
1 0 4	18.543	4.7810	100.0
2 0 0	20.599	4.3082	14.9
1 3 2	21.355	4.1574	34.1
2 1 1	21.726	4.0872	24.2
1 2 4	21.772	4.0787	24.3
2 1 2	22.746	3.9062	16.4
1 3 3	23.057	3.8542	45.4
2 2 0	23.559	3.7732	17.4
2 1 3	24.356	3.6515	17.1
1 2 5	24.707	3.6004	14.1
0 2 6	25.876	3.4403	17.1
1 3 5	27.848	3.2010	22.0
2 3 3	29.289	3.0467	19.9
1 3 6	30.741	2.9061	15.1
2 3 4	31.080	2.8751	15.1
1 6 1	36.195	2.4797	15.4

Table 2. Crystallographic data for **1**

Empirical formula	$H_6B_2O_{12}P_8$
Formula mass	467.43
Crystal size	0.7 × 0.7 × 0.7 mm
Temperature	−90(1) °C
Wavelength	λ(Mo-K_α) = 0.71073 Å
Detector distance	3 cm
Exposure time	10 s
Scan type, width	ω, 0.3°
Exposures taken	1800
$2\theta_{max}$	65°
Crystal system	orthorhombic
Lattice parameters:	
Single crystal[a]	a = 8.606(3) Å
	b = 15.686(6) Å
	c = 22.960(9) Å
	V = 3099(2) Å^3
Powder[b]	a = 8.6163(2) Å
	b = 15.6350(3) Å
	c = 22.9882(5) Å
	V = 3096.8(1) Å^3
Space group	*Pbca* (no. 61)
Z	8
hkl range	h: −13 to 13; k: −23 to 23; l: −34 to 34
F(000)	1856
Density (calculated)	2.003 g cm^{-3}
Linear absorption coefficient	μ = 0.952 mm^{-1}
Transmission factors	0.3898 and 0.4991
Reflections collected	49064
Independent reflections	5604
Reflections observed [$I > 2\ \sigma(I)$]	4704
Parameters refined	224
Absorption correction	semiempirical (see text)
R_{int}	0.0465
R_1 (observed reflections)	0.0364
wR_2 (observed reflections)	0.0938
GOOF	1.072
Largest diff. peak and hole	0.762 and −0.318 e·Å^{-3}

[a] At −90 °C. [b] At 25 °C, refined.

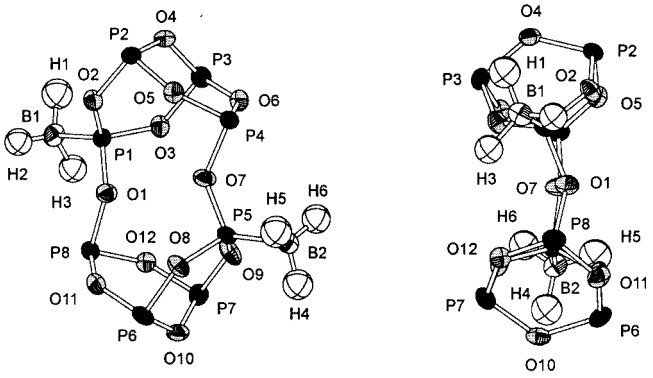

Figure 2. Molecular structure of **1** (two views; ellipsoids for 50% probability)

As there are no other phosphorus compounds known that have a similar structure, we are restricted to comparing the geometric parameters of **1** with those of P_4O_6X (X = O, S, Se) and $(RO)_3P{\cdot}BH_3$ (R = organic groups). The P−O bond lengths, varying between 157.8 and 167.1 pm, indicate pronounced P−O double-bond contributions [P−O (calculated): 176 pm;[32] P=O: 145.0 pm in P_4O_7,[3] 145.5 pm in P_4O_8 [4]] and may be subdivided into three types: P(B)−O_P^{III}, P^{III}−$O_{P(B)}$, and P^{III}−O_P^{III}, with P(B) and P^{III} being phosphorus atoms in the unit O_3PB and O_3P, respectively. The corresponding bond lengths reflect a characteristic distortion of the phosphorus−oxygen framework, which is already known from P_4O_6X (Table 3; X = O, S, Se) and is apparently induced by the electrophilic addition to the P_4O_6 cage. Thus, starting from the respective four-fold-coordinated phosphorus atom, the P−O bonds display an alternating contraction and elongation compared to the corresponding length in P_4O_6 (P−O: 165.3 pm[33]). But in the case of **1**, the distorting effect spreads out from two centers (P1 and P5) across a larger network. As mentioned in the introduction, the degree of this distortion so far seems to be rather independent of the nature of the terminal atom attached to the phosphorus atom. In this regard, the significant contraction of all P−O bonds by about 1 or 2 pm, as determined for **1**, is remarkable (Table 3). According to quantum chemical calculations,[26] the P(X)−O_P^{III} bonds are elongated, as the positive polarization of P(X) decreases, which on its part depends on the electron-withdrawing character of the attached element X. In contrast to these findings, boron generates significantly shorter P−O bonds than the more electronegative elements oxygen, sulfur, and selenium. A possible explanation for this observation may be seen in the fact that, contrary to chalcogen atoms, BH_3 groups are σ-acceptors with strongly reduced π-donor capabilities. A small degree of π-back donation by BH_3 was postulated very early in the investigations of the bonding in $PF_3{\cdot}BH_3$ [34,35] and $CO{\cdot}BH_3$.[34,36] More recent theoretical studies including natural energy decomposition analyses seem to confirm the effect of hyperconjugation for $CO{\cdot}BH_3$ [37,38] and $PF_3{\cdot}BH_3$.[39,40] On the other hand, it has to be stated that hyperconjugation is not mentioned in some of the respective treatments[41] and experimental evidence for it can hardly be provided. Anyway, the efficiency of π-back donation should be smaller for BH_3 than for chalcogen atoms leading, in the case of **1**, to an enhanced positive polarization of P(X). Another special feature of **1** arises from the head−tail linkage in combination with the alternation of contracted and stretched P−O bonds. As a result, both $P_4O_5{\cdot}BH_3$ units are connected by extremely asym-

Table 3. Mean bond lengths [pm] and mean bond angles [°] for **1**, P_4O_7, P_4O_6S, and P_4O_6Se; X = B, O, S, Se; P(X) = P in unit O_3PX; P^{III} = P in unit O_3P

	$P_8O_{12}{\cdot}2BH_3$	P_4O_7 [a]	P_4O_6S [b]	P_4O_6Se [c]
P(X)−O_P^{III}	158.3	159.4	159.6	160.2
P^{III}−$O_{P(X)}$	166.3	168.4	167.8	167.3
P^{III}−O_P^{III}	162.9	164.6	163.7	163.6
X−P(X)−O	115.2	114.9	115.3	115.8
O−P(X)−O	103.2	103.5	103.1	102.5
O−P^{III}−O	99.2	98.9	98.9	99.0
P(X)−O−P^{III}	132.7	123.9	124.2	124.6
P^{III}−O−P^{III}	132.9	128.1	128.1	128.0

[a] Refs.[2,3] [b] Ref.[7] [c] Ref.[11]

metrical P−O−P bridges, containing the longest and the two shortest P−O bonds in the molecule (167.1, 158.0, and 157.8 pm, respectively). These bridges are arranged in a way that favors a symmetrical cleavage of the molecule. In fact, this is what we have observed in both, solution (^{31}P NMR spectra) and gas phase (mass spectra).

The O−P−O bond angles ranging from 95.3 to 104.7° tend to be about 4° smaller at the P^{III} than at the P(X) atom (Table 3). The mean bond angles for O−P−O and X−P−O are nearly identical to those in P_4O_6X (Table 3), whereas the mean values for P−O−P are substantially larger [about 5° for P^{III}−O−P^{III} and about 9° for P(X)−O−P^{III}]. Both, contraction of P−O bonds and widening of P−O−P bond angles, are consistent with assuming an increased double-bond character. These π-interactions are promoted by a reduction of ring strain upon dimerization, and balance the positive polarization of the P(B) atom at the same time.

The geometric parameters within the $O_3P{\cdot}BH_3$ unit of **1** correspond quite well with the values obtained for borane complexes of organic phosphites $(RO)_3P{\cdot}BH_3$.[42−45] The P−B mean bond length of 187.0 pm, especially, is in line with assuming a pure single bond. Due to the difficulties in accurately localizing hydrogen positions by X-ray diffraction methods, the B−H bond lengths and bond angles vary significantly (mean values for B−H: 109.8 pm; P−B−H: 103.5°). However, the H−B−H mean bond angle of 114.7° is exactly the average value of 109.4 and 120°, encountered for tetrahedral and trigonal-planar coordination of the boron center, respectively. The intermolecular atomic distances are in the range as expected for van der Waals interactions.

NMR Spectroscopy

In our previous investigations on phosphorus oxides and their derivatives, NMR spectroscopy turned out to be a useful tool, sometimes providing essential insights otherwise not accessible.[46−48] For **1** the isotropic signals of nearly all eight crystallographically independent phosphorus atoms can be resolved in the ^{31}P MAS NMR spectrum (Figure 3).

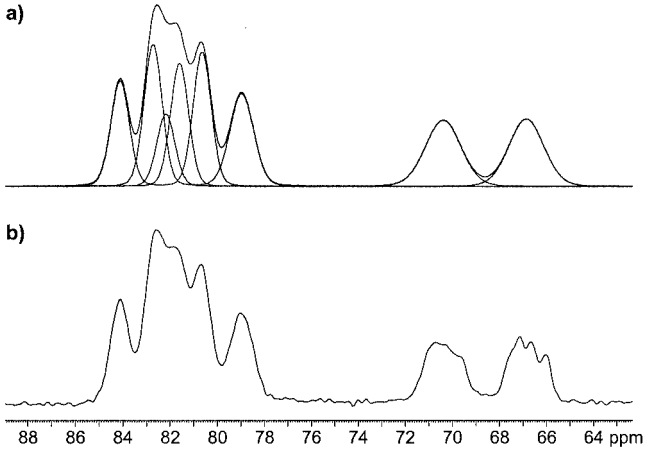

Figure 3. Isotropic signals of the ^{31}P MAS NMR spectrum of **1**; simulated with deconvolution (a; see Table 4) and observed (b)

Table 4. Simulation parameters for the isotropic ^{31}P MAS NMR signals of **1** (see Figure 3)

δ [ppm]	Amplitude	Line width [Hz]	Intensity [%]
66.9	73.5	279.6	13.4
70.4	72.1	286.2	13.5
79.0	101.0	190.4	12.6
80.7	146.9	145.8	14.0
81.6	134.6	145.4	12.9
82.2	79.0	145.8	7.6
82.8	155.2	145.8	14.9
84.2	115.1	145.7	11.1

A simulation using the individual chemical shifts given in Table 4 is in good agreement with the observed spectrum (Figure 3). By means of cross polarization from ^{1}H onto ^{31}P spins the signals at δ = 66.9 and 70.4 ppm could be assigned to the BH_3-bearing phosphorus atoms P1 and P5. This is in accordance with additional broadening and splitting of these signals due to coupling with ^{11}B nuclei having a quadrupole moment. Thus, the other six signals can be attributed to the P2, P3, P4, P6, P7, and P8 atoms. A further assignment to individual atoms has not been attempted. An explanation for the low signal intensity at δ = 82.2 ppm cannot be given. The isotropic chemical shifts of the BH_3 groups of **1**, observed in ^{1}H and ^{11}B MAS NMR spectra, are δ = 0.88 and −39.6 ppm, respectively, and match quite well with the values of $P_4O_6{\cdot}BH_3$ (δ = 0.6 and −40 ppm[29]).

The NMR spectra of **1**, in solution, are in accordance with molecules exhibiting C_{2h} symmetry. This observation might be understood by assuming a flexible P_8O_{12} framework allowing fast internal motion in solution, and adaptation to packing requirements in the solid phase. In the case of fluctuations being faster than the time-scale of the NMR spectroscopic experiments, a time-averaged state of the molecule is recorded instead of an individual conformer. As a consequence, the P1 and P5 atoms appear as chemically equivalent, but magnetically inequivalent nuclei. The same holds for P4 and P8 and for P2, P3, P6, and P7, respectively giving an AA′BB′B′′B′′′XX′ spin system. Therefore, a set of three signals is obtained in the ^{31}P NMR spectrum (Figure 4). P1 and P5 give rise to a signal appearing as a diffuse hump at δ = 71.5 ppm due to the quadrupole moment of the boron atom and complicated spin-spin coupling with hydrogen, boron, and trivalent phosphorus

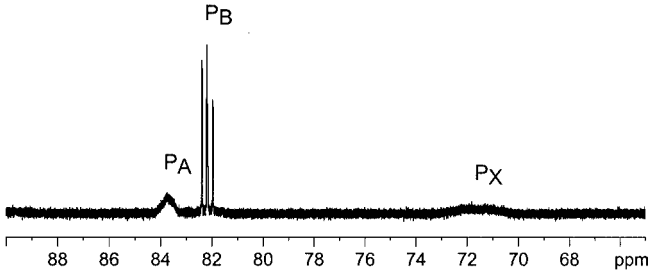

Figure 4. ^{31}P NMR spectrum of dissolved **1** at 23 °C

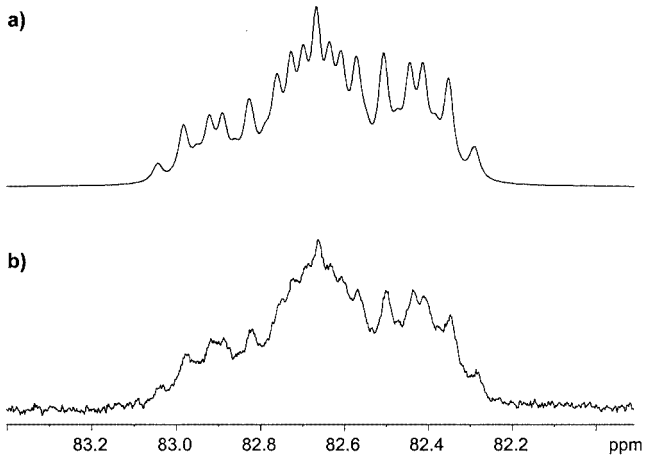

Figure 5. Splitting pattern for P_A in the ^{31}P NMR spectrum of dissolved **1**; simulated (a; see Table 5) and observed at −20 °C (b)

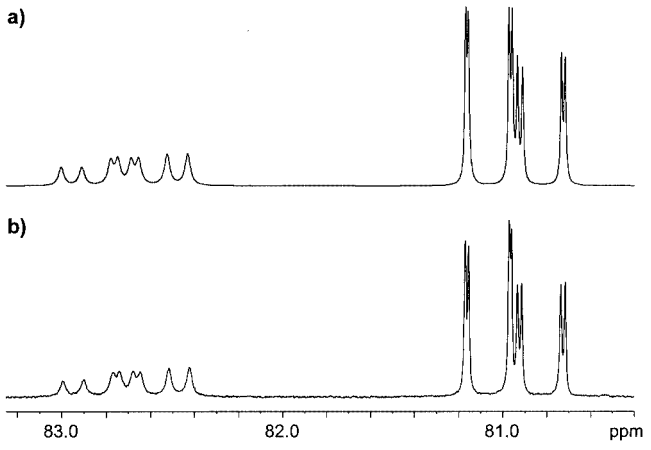

Figure 6. Splitting patterns for P_A and P_B in the $^{31}P\{^1H\}$ NMR spectrum of dissolved **1**; simulated (a; see Table 5) and observed at −20 °C (b)

atoms. The best resolution for the splitting pattern of the broad signal at δ = 83.7 ppm has been obtained at −20 °C for the temperature-dependent measurements (Figure 5; the displacement of the signal is caused by the general temperature dependence of chemical shifts). The corresponding $^{31}P\{^1H\}$ NMR signal (Figure 6) indicates pronounced ^{31}P-^1H coupling, whereas the other signals remain unchanged. The splitting patterns for both NMR spectra can be explained and simulated in full detail using the parameters summarized in Table 5 (Figures 5 and 6). The assignments are consistent with homonuclear decoupling experiments and an intensity ratio of 1:2:1 for the signals of P_A, P_B, and P_X, respectively.

In line with increased P−O double-bond contributions as discussed above, a considerable upfield shift is to be expected for the ^{31}P NMR signals of **1** in comparison with its monomeric counterpart $P_4O_6{\cdot}BH_3$ (the upfield shifts for the BH_3-bearing and for the trivalent phosphorus atoms are about 20 and 40 ppm, respectively; see Exp. Sect.). Among molecular phosphorus oxides and their derivatives only the trivalent phosphorus atoms of $P_4O_6X_3$ (X = O, S, Se; also mixed) exhibit chemical shifts in this region. Surprisingly, the coupling constants are nearly unaffected by the change in bonding situation. Thus, the coupling constants within the bicyclic $P_4O_5{\cdot}BH_3$ unit ($^2J_{AB}$ = 29.2; $^2J_{BX}$ = 24.0 Hz) are of the same order as the $^2J_{P,P}$ values, found for $P_4O_6{\cdot}BH_3$ (27.7 Hz) and $P_4O_6{\cdot}2BH_3$ (24.5 Hz). The weak coupling across P1−O1−P8 and P4−O7−P5 ($^2J_{AX}$ = 11.4 Hz) reflects the flexible linkage between the $P_4O_5{\cdot}BH_3$ subunits. The additional quadruplet splitting of the P_A signal, observed in the ^{31}P NMR spectrum (Figure 5), may be considered as either $^4J_{AH}$ or $^6J_{AH}$. Having the flexible linkages in mind, coupling along the rigid $P_4O_5{\cdot}BH_3$ units ($^6J_{AH}$) seems to be more favorable.

Vibrational Spectroscopy

On dimerization, the molecular symmetry of $P_4O_6{\cdot}BH_3$ (C_{3v}) is reduced to at least C_{2h}, leading to the splitting of vibrational modes of the *E* representation. Moreover, the distortion of the P_8O_{12} cage in the crystalline solid provokes a further symmetry reduction to C_1, which is confirmed by the violation of the mutual exclusion rule normally holding for centrosymmetric molecules. Thus, absorptions at 431, 655, 666, 757, 1119, 2343, and 2363 cm^{-1} are observed in both, IR and Raman spectra (Figure 7; Table 6). As expected, the spectra are very similar to those of P_4O_6 [49] and P_4O_7,[3] for which strong bands around 950 cm^{-1} in the IR spectrum (broad) and around 620 cm^{-1} in the Raman spectrum (sharp) are quite characteristic. The vibrational frequencies of **1** are shifted by up to 20 cm^{-1} compared to

Table 5. Simulation parameters for the ^{31}P NMR spectrum of dissolved **1** (see Figures 5 and 6)

Molecular symmetry	C_{2h}		
Spin system	AA′BB′B′′B′′′XX′		
Spectrometer type	300 MHz		
Frequency	121.5008 MHz		
Nuclei	δ [ppm]		Line width [Hz]
P_A: P4, P8	82.65		3.5
P_B: P2, P3, P6, P7	80.95		1.2
P_X: P1, P5	70.5		1.2
H	0.8		0.3
Coupling constants [Hz]			
$^2J_{AB}$: J_{24}, J_{34}, J_{68}, J_{78}	29.2	$^2J_{BX}$: J_{12}, J_{13}, J_{56}, J_{57}	24.0
$^2J_{AX}$: J_{18}, J_{45}	11.4	J_{AH}: J_{4H}, J_{8H}	7.5

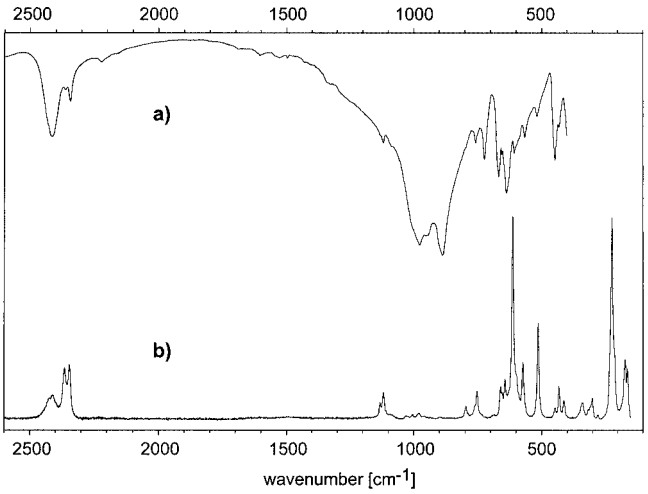

Figure 7. IR (a) and Raman (b) spectrum of solid **1**

those of P_4O_6 and P_4O_7 (Table 6). As cage vibrations are always mixed with motions of the terminally bonded groups, which is different for P_4O_7 and **1**, reliable conclusions concerning the nature of the P−O cage bonds cannot be drawn from the comparison of individual frequencies at a first glance. The four absorptions ranging from 2340 to 2430 cm^{-1} may be attributed to symmetric and antisymmetric B−H stretching modes and agree with data of compounds containing similar P−BH_3 groups.[42,50] The region in which ν(P−B) modes are observed for $R_3P{\cdot}BH_3$ (R = H, Me, Cl),[50] is between 560 and 585 cm^{-1}. Pronounced bands at 565 and 574 cm^{-1} are obtained in the IR and Raman spectra of **1** and are not significant in the spectra of P_4O_6 and P_4O_7. Therefore, assigning them as ν(P−B) seems to be reasonable.

Table 6. Vibrational frequencies [cm^{-1}] observed in the IR and Raman spectra of solid **1** (see Figure 7), P_4O_7, and P_4O_6

$P_8O_{12}{\cdot}2BH_3$		P_4O_7 [a]		P_4O_6 [b]	
IR	Raman	IR	Raman	IR	Raman
	162 m				
	171 m				
	215 s,sh				
	224 vs				
	279 vw	266 m	269 m		285 vw
	301 m	299 m	306 m	302 vw	302 m
	310 w, sh	314 w			
	317 w, sh	323 w	333 w		
	342 m	353 vw			
	413 m	392 vw	392 m	407 vs	407 m
431 m, sh	433 m	427 m	429 m		
446 s	448 w				
518 w	515 s	532 m	534 m		
		554 vw			570 w
565 m, P−B	574 m, P−B				
607 m	600 m, sh				
	614 vs	615 m	625 vs		614 vs
636 s	644 m	635 sh		644 vs	644 s
655 m	655 m, sh	653 w	657 m		
666 s	661 m	667 sh			
		674 w			673 w
		695 vw			
723 s		711 m	708 vw		
757 m	753 m				
	762 w, sh				
	797 w	781 w			
886 vs, br					
947 vs, sh		930 sh	935 vw	921 vs	921 vw
975 vs, br	981 vw	965 vs, br	960 vw		
	1005 vw				
1119 m, sh	1120 m				
	1133 w				
		1345 s	1333 m		
1496 vw					
1530 vw					
1604 vw					
1687 vw					
2224 w					
2343 m, B−H	2346 m, B−H				
2363 m, B−H	2366 m, B−H				
2417 s, B−H	2412 w, B−H				
	2426 w, sh, B−H				

[a] Ref.[3] [b] Refs.[49,3]

Mass Spectrometry

Some instructive conclusions can be drawn about the nature of the P_8O_{12} cage from mass spectrometry. The corresponding data for **1** are given in the Exp. Sect. Boron-containing species are easily identified by their characteristic isotope patterns, which are modified by consecutive hydrogen abstraction from BH_3 groups. In contrast to the molecular ions almost not being detected at all, peaks with intensities around 13% are observed in the EI mass spectrum at 100 °C arising from P_8O_{12} and $P_8O_{12}{\cdot}BH_3$. MS/MS experiments could not be used to decide whether the corresponding BH_3 abstraction occurs before ionization or afterwards, due to the low intensity of the molecular ion peak. Nevertheless, the differing peak intensities for P_8O_{12}-containing species suggest an enhanced stability for P_8O_{12} and $P_8O_{12}{\cdot}BH_3$ ions. In addition, the three P_8O_{12}-containing species show different fragmentation behaviors. Thus, the P_8O_{12} cage of **1** is cleaved symmetrically yielding mainly P_4O_6 and $P_4O_6{\cdot}BH_3$ [MS (EI, 40 °C): *m/z* = 220 and 233, respectively; Exp. Sect.), whereas for $P_8O_{12}{\cdot}BH_3$ the cleavage takes place asymmetrically (MS of $P_8O_{12}{\cdot}BH_3^+$; Exp. Sect.), resulting in an enhanced formation of $P_4O_7{\cdot}BH_2^+$ in the EI mass spectrum of **1** at 100 °C (*m/z* = 249; Exp. Sect.). For $P_8O_{12}^+$ both, symmetrical and asymmetrical cleavage, occur to the same extent generating $P_4O_5^+$ and $P_4O_6^+$ (MS of $P_8O_{12}^+$; Exp. Sect.). The increased stability of P_8O_{12} and $P_8O_{12}{\cdot}BH_3$ compared to **1** is supported by further observations. Because Chemical Ionization (CI) is less destructive than Electron Impact (EI), the cleavage of $P_8O_{12}{\cdot}BH_3$ is drastically reduced, whereas that of **1** is boosted (cf. peak intensity ratio of *m/z* = 233 and 249 for MS (EI, 100 °C) and MS (CI, 100 °C); Exp. Sect.). In the absence of collision gas no cleavage is detected at all for $P_8O_{12}^+$, even at 100 °C. Both, the different stabilities and fragmentation patterns may be fully understood from the results of the crystal structure determination. Due to the formation of asymmetrical P1−O−P8 and P4−O−P5

bridges, the complexation of borane groups at P1 and P5 destabilizes the P_8O_{12} cage of **1** and induces symmetrical cleavage. On the other hand, in P_8O_{12} the two bicyclic P_4O_5 units are connected by symmetrical P−O−P bridges stabilizing the framework and permitting symmetrical as well as asymmetrical cleavage, at the same time. Finally, $P_8O_{12}{\cdot}BH_3$ is destabilized by only one asymmetrical P−O−P linkage. These results encourage further investigations aiming at the synthesis of dimeric phosphorus oxides. Selective BH_3 abstraction cannot be accomplished by thermal degradation, for example by heating solid **1** for some days at 90 °C. The decomposition product thus obtained is an amorphous orange solid, which is insoluble in toluene.

Conclusion

The thermodynamic driving force of the dimerization of $P_4O_6{\cdot}BH_3$ consists in a gain of enthalpy due to additional P−O double-bond contributions within the P_8O_{12} cage. These are promoted by a relief of angular strain and are in line with contracted P−O bonds (about 20 pm per P_4O_6 unit), enlarged P−O−P bond angles, and enhanced electronic shielding of phosphorus nuclei in **1**. At low temperatures, the benefit in enthalpy compensates for the loss in entropy, associated with dimerization. As the solubility of dimeric species is lower than that of $P_4O_6{\cdot}BH_3$, **1** is continuously removed from the solution through crystallization. As a result, the solved $P_4O_6{\cdot}BH_3$ dimerizes selectively in a kinetically controlled reaction in the absence of nucleophilic reagents. The poor π-donor property of BH_3 is responsible for the different reactivity of $P_4O_6{\cdot}BH_3$, compared to other P_4O_6 derivatives. The additional double-bond contributions within P(B)−O, balancing the positive polarization at the fourfold-coordinated phosphorus atom P(B) at the expense of the adjacent $P^{III}-O_{P(B)}$ bonds, strongly favor the fission of one of the destabilized $P^{III}-O_{P(B)}$ bonds. In this respect, the behavior of the $H_3B-P(OP)_3$ group would be very similar to that of alkylated phosphites $[R'-P(OR)_3]^+$, which are immediately cleaved in the well-known Michaelis−Arbuzov reaction[51−53] yielding organic phosphonates $R'-PO(OR)_2$. If the resulting polarities are taken into account, intermolecular recombination of the dangling P−O bonds create molecules having exactly the constitution observed for **1** (head−tail linkage). But, of course, a concerted mechanism via a four-membered P−O−P−O ring including two intact $P_4O_6{\cdot}BH_3$ units is also a reasonable alternative. This type of ring-opening reaction is considered as one possible pathway for the cationic polymerization of cyclosiloxanes.[54] In any case, the electrophilic addition of BH_3 seems to be associated with kinetic activation of the P_4O_6 cage.

Experimental Section

General: Synthesis of **1** as well as all sample preparations were carried out under inert conditions (argon) either in a glass apparatus or in a glove box. P_4O_6 (Hoechst) was purified by distillation at 50 °C under reduced pressure into a cooling trap. Toluene was heated under reflux over P_4O_{10} and freshly distilled prior to use. $Me_2S{\cdot}BH_3$ was commercially available (Strem Chemicals; about 5% excess of Me_2S).

Synthesis: $Me_2S{\cdot}BH_3$ (0.47 mL, 0.38 g, 4.96 mmol) was added dropwise to a solution of P_4O_6 (1.2 g, 5.46 mmol) in toluene (1.0 mL) at 0 °C while stirring. The clear colorless solution was stirred at 0 °C for a further 2 h and Me_2S was subsequently removed in vacuo at −10 °C over 4 min. At this stage the solution contained mainly $P_4O_6{\cdot}BH_3$ with small amounts of P_4O_6, $P_4O_6{\cdot}2BH_3$, P_4O_7, and P_4. After storage for three months at −30 °C the almost solidified solution was warmed up to room temperature. Clear colorless crystals of **1**, which were up to 1 mm in size and cuboid in shape, initially remained undissolved. The crystals were separated from the mother liquor at 0 °C and dried in vacuo at room temperature for 5 h giving pure **1** (yield: ca. 0.38 g, 0.82 mmol, 30%). The reproducibility of the crystallization strongly depends on temperature and concentration. The best results were obtained for concentrations ranging from 1.25 to 1.43 mg of P_4O_6 per mL of toluene (after removal of Me_2S and some solvent in vacuo).

Caution: Solid $P_8O_{12}{\cdot}2BH_3$ is highly explosive when exposed to any kind of mechanical stress, even under inert conditions at −80 °C (friction- and shock-sensitive). Contact with pure water or ethanol causes violent decomposition. We recommend that the solid should be neither handled in sealed glass vessels nor in large amounts (maximum 1.5 g). Under argon, loose crumbs can be ground without danger, if portions less than 100 mg are used. For disposal, **1** is covered with aromatic solvents and carefully decomposed by adding ethanol in small portions (formation of H_2).

Crystal Structure Analysis: A cuboid crystal with dimensions given in Table 2 was picked up by a mounted CryoLoop (Hampton Research) using an inert immersion oil (Hampton Research) and then measured at −90 °C using a SMART 1000 diffractometer with CCD detector and graphite monochromator (Bruker AXS). Absorption corrections based on symmetry-equivalent and redundant reflections (SADABS); structure solution by direct methods (SHELXS-97[55]); structure refinement according to full-matrix least-squares procedures against F^2 (SHELXL-97[56]); hydrogen atoms refined freely (isotropic); display of molecular structure by DIAMOND.[57] Further details of the crystal structure investigation may be obtained from Table 2 and from the Fachinformationszentrum Karlsruhe, 76344 Eggenstein-Leopoldshafen, Germany [Fax: (internat.) + 49-7247/808-666; E-mail: crysdata@fiz-karlsruhe.de], on quoting the depository number CSD-411904 and the names of the authors.

Powder Diffractometry: Stadi P diffractometer (Stoe & Cie); Debye−Scherrer geometry; Ge single crystal (111) as monochromator; $\lambda(\text{Cu-}K_{\alpha 1}) = 154.0598$ pm; **1** was ground in a glove box and sealed in a capillary (Hilgenberg) with 0.2 mm in diameter; after zero point correction on the basis of silicon as external standard and baseline correction profile fitting was performed by FULLPROF98[58] using least-squares procedures; refinement results are given in Table 1 (reflection positions) and Table 2 (lattice parameters).

NMR Spectroscopy: Solutions: 300 MHz spectrometer (Avance DPX 300 SB; Bruker); 121.50 MHz (^{31}P), 96.29 MHz (^{11}B); in toluene; [D_6]benzene or [D_8]toluene as lock solvents; glass tubes (Wilmad) were sealed; simulation by WINDAISY.[59] Solid: 400 MHz spectrometer (Avance DSX 400 WB; Bruker); 2.5 mm CP MAS

probe; 161.98 (^{31}P), 128.38 (^{11}B), 400.12 MHz (^{1}H); simulation by WINFIT;[60] 85% phosphoric acid, tetramethylsilane, and $(C_2H_5)_2O{\cdot}BF_3$ as external standards with upfield being negative; display of spectra by WINNMR.[61] **$P_4O_6{\cdot}BH_3$:** $^{11}B\{^1H\}$ NMR: $\delta = -39.6$ [d, $^1J_{PB} = 57$ Hz, 1 B, P*B*H$_3$] ppm. ^{31}P NMR: $\delta = 90.0$ [broad, 1 P, O$_3$*P*B], 117.1 [dq, $^2J_{P,P} = 27.7$, $^4J_{PH} = 0.7$ Hz, 3 P, O$_3$*P*] ppm. **$P_4O_6{\cdot}2BH_3$:** $^{11}B\{^1H\}$ NMR: $\delta = -40.2$ [d, $^1J_{PB} = 53$ Hz, 2 B, P*B*H$_3$] ppm. ^{31}P NMR: $\delta = 98.4$ [broad, 2 P, O$_3$*P*B], 117.4 [t, $^2J_{P,P} = 24.5$ Hz, 2 P, O$_3$*P*] ppm.

IR and Raman Spectroscopy: FT-IR spectrometer IFS 113v (Bruker); Genzel interferometer; KBr pellet (decomposition within CsI). FT-Raman spectrometer LabRam system (Jobin Yvon); He-Ne LASER (632.817 nm); sample sealed in a silica capillary.

Mass Spectrometry: Triple-quadrupole mass spectrometer TSQ 700 (Finnigan MAT); direct inlet; heatable sample holder; ionization at 150 °C. MS (EI, 70 eV, 40 °C): *m/z* (%) = 47 (48) $[PO]^+$, 95 (13) $[P_2O_2H]^+$, 123 (16) $[P_2O_3{\cdot}BH_2]^+$, 157 (81) $[P_3O_4]^+$, 173 (13) $[P_3O_5]^+$, 185 (7) $[P_4O_3{\cdot}BH_2]^+$, 204 (67) $[P_4O_5]^+$, 220 (100) $[P_4O_6]^+$, 233 (33) $[P_4O_6{\cdot}BH_2]^+$, 249 (8) $[P_4O_7{\cdot}BH_2]^+$, 440 (< 1) $[M - 2\,BH_3]^+$, 452 (1) $[M - BH_3 - H_2]^+$. MS (EI, 70 eV, 100 °C): *m/z* (%) = 47 (86) $[PO]^+$, 94 (20) $[P_2O_2]^+$, 123 (16) $[P_2O_3{\cdot}BH_2]^+$, 141 (13) $[P_3O_3]^+$, 157 (100) $[P_3O_4]^+$, 173 (24) $[P_3O_5]^+$, 185 (20) $[P_4O_3{\cdot}BH_2]^+$, 204 (82) $[P_4O_5]^+$, 220 (85) $[P_4O_6]^+$, 233 (29) $[P_4O_6{\cdot}BH_2]^+$, 249 (94) $[P_4O_7{\cdot}BH_2]^+$, 267 (83) $[P_5O_7]^+$, 283 (37) $[P_5O_8]^+$, 311 (12) $[P_5O_9{\cdot}BH]^+$, 359 (9) $[P_7O_8{\cdot}BH_3]^+$, 440 (13) $[M - 2\,BH_3]^+$, 452 (13) $[M - BH_3 - H_2]^+$, 464 (< 1) $[M - 2\,H_2]^+$. MS (CI, methane, 3−9 Torr, 100 °C): *m/z* (%) = 92 (13) $[P_2O{\cdot}BH_3]^+$, 111 (10) $[P_2O_3H]^+$, 125 (23) $[P_3O_2]^+$, 157 (76) $[P_3O_4]^+$, 173 (13) $[P_3O_5]^+$, 205 (54) $[P_4O_5H]^+$, 220 (72) $[P_4O_6]^+$, 233 (100) $[P_4O_6{\cdot}BH_2]^+$, 249 (31) $[P_4O_7{\cdot}BH_2]^+$, 267 (15) $[P_5O_7]^+$, 285 (8) $[P_4O_{10}H]^+$, 441 (4) $[M + H - 2\,BH_3]^+$, 453 (26) $[M + H - BH_3 - H_2]^+$. MS of $P_8O_{12}{\cdot}BH_3^+$ (**1** as source compound at 80 °C): *m/z* (%) = 249 (90) $[P_4O_7{\cdot}BH_2]^+$, 454 (100) $[P_8O_{12}{\cdot}BH_3]^+$. MS of $P_8O_{12}^+$ (**1** as source compound at 100 °C, argon as collision gas): *m/z* (%) = 204 (20) $[P_4O_5]^+$, 220 (20) $[P_4O_6]^+$, 440 (100) $[P_8O_{12}]^+$ (without collision gas no fragmentation was observed).

Acknowledgments

We are grateful to Hoechst AG (Knapsack, Germany) for the generous supply of P_4O_6.

[1] K. H. Jost, M. Schneider, *Acta Crystallogr., Sect. B* **1981**, *37*, 222.
[2] M. Jansen, M. Voss, *Angew. Chem.* **1981**, *93*, 120, *Angew. Chem. Int. Ed. Engl.* **1981**, *20*, 100.
[3] M. Möbs, M. Jansen, *Z. Anorg. Allg. Chem.* **1984**, *514*, 39.
[4] S. Strojek, M. Jansen, *Z. Naturforsch., Teil B* **1997**, *52*, 906.
[5] B. Lüer, M. Jansen, *Z. Kristallogr.* **1991**, *197*, 247.
[6] M. Jansen, B. Lüer, *Z. Kristallogr.* **1986**, *177*, 149.
[7] F. Frick, M. Jansen, P. J. Bruna, S. D. Peyerimhoff, *Chem. Ber.* **1991**, *124*, 1711.
[8] F. Frick, M. Jansen, *Z. Anorg. Allg. Chem.* **1993**, *619*, 281.
[9] F. Frick, M. Jansen, *Z. Kristallgr.* **1994**, *209*, 985.
[10] F. Frick, PhD Thesis, Univ. Bonn, **1993**.
[11] J. Clade, M. Jansen, B. Engels, C. M. Marian, *Z. Anorg. Allg. Chem.* **1995**, *621*, 2065.
[12] M. Jansen, A. Tellenbach, *Z. Anorg. Allg. Chem.* **1998**, *624*, 1267.
[13] J. Clade, M. Jansen, *Z. Anorg. Allg. Chem.* **1996**, *622*, 1630.
[14] J. Clade, PhD Thesis, Univ. Bonn, **1996**.
[15] J. G. Riess, J. R. Van Wazer, *J. Am. Chem. Soc.* **1966**, *88*, 2166.
[16] E. D. Pierron, P. J. Wheatley, J. G. Riess, *Acta Crystallogr.* **1966**, *21*, 288.
[17] M. L. Walker, J. L. Mills, *Inorg. Chem.* **1975**, *14*, 2438.
[18] M. Jansen, J. Clade, *Acta Crystallogr., Sect. C* **1996**, *52*, 2650.
[19] M. L. Walker, J. L. Mills, *J. Organomet. Chem.* **1976**, *120*, 355.
[20] J. G. Riess, J. R. Van Wazer, *Inorg. Chem.* **1966**, *5*, 178.
[21] M. Loeper, U. Schülke, *Z. Anorg. Allg. Chem.* **1983**, *500*, 40.
[22] U. Schülke, *Phosphorus, Sulfur Silicon* **1990**, *51/52*, 153.
[23] M. Jansen, S. Strojek, *J. Chem. Soc., Chem. Commun.* **1995**, 1509.
[24] S. Strojek, M. Jansen, *Chem. Ber.* **1996**, *129*, 121.
[25] S. Strojek, PhD Thesis, Univ. Bonn, **1998**.
[26] M. Mühlhäuser, B. Engels, C. M. Marian, S. D. Peyerimhoff, P. J. Bruna, M. Jansen, *Angew. Chem.* **1994**, *106*, 578; *Angew. Chem. Int. Ed. Engl.* **1994**, *33*, 563.
[27] G. Kodama, H. Kondo, *J. Am. Chem. Soc.* **1966**, *88*, 2045.
[28] J. G. Riess, J. R. Van Wazer, *J. Am. Chem. Soc.* **1966**, *88*, 2339.
[29] J. G. Riess, J. R. Van Wazer, *J. Am. Chem. Soc.* **1967**, *89*, 851.
[30] A. Tellenbach, M. Jansen, *Angew. Chem.* **2001**, *113*, 4838; *Angew. Chem. Int. Ed.* **2001**, *40*, 4691.
[31] W. Eiserbeck, P. Neumann, U. Schülke, M. Meisel, *Phosphorus, Sulfur Silicon* **1994**, *93/94*, 373.
[32] L. Pauling, *The Nature of the Chemical Bond*, Cornell University Press, Ithaca − New York, **1948**, p. 160−167.
[33] M. Jansen, M. Möbs, *Inorg. Chem.* **1984**, *23*, 4486.
[34] K. F. Purcell, *Inorg. Chem.* **1972**, *11*, 891.
[35] I. H. Hillier, J. C. Marriott, V. R. Saunders, M. J. Ware, D. R. Lloyd, N. Lynaugh, *J. Chem. Soc., Chem. Commun.* **1970**, 1586.
[36] D. R. Lloyd, N. Lynaugh, *J. Chem. Soc., Chem. Commun.* **1970**, 1545.
[37] E. D. Glendening, A. Streitwieser, *J. Chem. Phys.* **1994**, *100*, 2900.
[38] C. W. Bauschlicher, A. Ricca, *Chem. Phys. Lett.* **1995**, *237*, 14.
[39] H. Anane, A. Jarid, A. Boutalib, I. Nebot-Gil, F. Tomás, *Chem. Phys. Lett.* **2000**, *324*, 156.
[40] C. Loschen, K. Voigt, J. Frunzke, A. Diefenbach, M. Diedenhofen, G. Frenking, *Z. Anorg. Allg. Chem.* **2002**, *628*, 1294.
[41] I. Røeggen, *Chem. Phys.* **1992**, *162*, 271.
[42] J. C. Clardy, D. S. Milbrath, J. G. Verkade, *Inorg. Chem.* **1977**, *16*, 2135.
[43] S. Cserepi-Szucs, I. Toth, L. Parkanyi, J. Bakos, *Tetrahedron* **1998**, 3135.
[44] Y. Yamanoi, T. Imamoto, *J. Org. Chem.* **1997**, *62*, 8560.
[45] T. Imamoto, E. Nagato, Y. Wada, H. Masuda, K. Yamaguchi, T. Uchimaru, *J. Am. Chem. Soc.* **1997**, *119*, 9925.
[46] W. Hoffbauer, S. Wefing, G. Klösters, F. Frick, M. Jansen, *Solid State Nucl. Magn. Reson.* **1999**, *14*, 211.
[47] G. Jeschke, W. Hoffbauer, M. Jansen, *Chem. Eur. J.* **1998**, *4*, 1755.
[48] U. Fleischer, F. Frick, A. R. Grimmer, W. Hoffbauer, M. Jansen, W. Kutzelnigg, *Z. Anorg. Allg. Chem.* **1995**, *621*, 2012.
[49] A. R. S. Valentim, B. Engels, S. D. Peyerimhoff, J. Clade, M. Jansen, *J. Phys. Chem.* **1998**, *A102*, 3690.
[50] J. Weidlein, U. Müller, K. Dehnicke, *Schwingungsfrequenzen I − Hauptgruppenelemente*, Georg Thieme, Stuttgart − New York, **1981**.
[51] B. A. Arbuzov, *Pure Appl. Chem.* **1964**, *9*, 307.
[52] R. G. Harvey, E. R. De Sombre, *Top. Phosphorus Chem.* **1964**, *1*, 61.
[53] R. F. Hudson, *Structure and Mechanism in Organophosphorus Chemistry*, Academic Press, London, **1965**.
[54] R. Bischoff, P. Sigwalt, *Polym. Int.* **1996**, *40*, 99.
[55] G. M. Sheldrick, *SHELXS-97*, Univ. Göttingen, Germany, **1997**.
[56] G. M. Sheldrick, *SHELXL-97*, Univ. Göttingen, Germany, **1997**.
[57] K. Brandenburg, *DIAMOND*, version 2.1a, Bonn, Germany, **1999**.
[58] J. Rodriguez-Carvajal, *FULLPROF98*, version 0.2, Laboratoire Leon Brillouin, France, **1998**.
[59] *WINDAISY*, version 4.05, Bruker-Franzen Analytik GmbH, Germany.
[60] *WINFIT*, Bruker-Franzen Analytik, Germany.
[61] *WINNMR*, version 6.1, Bruker Daltonik, Germany, **1999**.
[62] Natl. Bur. Stand. (U. S.), Monogr. **1976**, *25*, 35.

Received April 15, 2003

